Six Degree-of-Freedom Haptic Simulation of Probing Dental Caries Within a Narrow Oral Cavity

Dangxiao Wang, *Senior Member, IEEE*, Xiaohan Zhao, Youjiao Shi, Yuru Zhang, *Senior Member, IEEE*, Jianxia Hou, and Jing Xiao, *Fellow, IEEE*

Abstract—Haptic simulation of handling pathological tissues is a crucial component to enhance virtual surgical training systems. In this paper, we introduce a configuration-based optimization approach to simulate the exploration and diagnosis of carious tissues in dental operations. To simulate the six Degree-of-Freedom (6DoF) haptic interaction between the dental probe and the oral tissues, we introduce two interaction states, the sliding state and the penetration state, which simulate the exploration on the surface of and inside of the caries, respectively. Penetration criteria considering a contact force threshold are defined to trigger the switch between the two states. By utilizing a simplified friction model based on the optimization approach, various multi-region frictional contacts between the probe and carious tissues are simulated. To simulate the exploration within the carious tissues for diagnosing the depth of the caries, *a dynamic sphere tree* is used to constrain the insertion/extraction of the probe within carious tissues along a fixed direction while enabling simulation of additional contacts of the probe with neighboring oral tissues during the insertion/extraction process. Experimental results show that decays with different levels of stiffness and friction coefficients can be stably simulated. Preliminary user studies show that users could easily identify the invisible boundary between the decay and healthy tissues and correctly rank the depth of target decays within a required time limit. The proposed approach could be used for training delicate motor skill of probing target carious teeth in a narrow oral cavity, which requires collaborated control of tool posture and insertion/extraction force, while avoiding damages to adjacent healthy tissues of the tongue and gingiva.

Index Terms—Haptic rendering, carious tissues, friction simulation, penetration force, extraction force, boundary simulation

1 Introduction

Haptic rendering of handling pathological tissues is important for enhancing the usability of surgical simulation and training systems. High-fidelity rendering involving fine physical features on or inside pathological tissues such as texture, friction and stiffness, may greatly enhance the experiences of trainees to get familiar with physical properties of various diseases, and thus to practice delicate motor skills required for diagnosis/treatment of these diseases.

1.1 Problem Statement

Diagnosing dental caries is a fundamental operation in clinical dental practices, which requires a dentist to detect subtle differences of stiffness and friction between carious and healthy tissues. During caries diagnosis operation, dentists slide the probe along the surface of a target tooth to detect decays or insert the probe's tip into carious tissues to measure its depth [1], [2], [3].

The first step of caries diagnosis task is to detect the location and severity level of the carious tissue, as well as the boundary between the carious and healthy tissues by haptic perception or combined haptic-visual perception. A dentist uses a dental probe to tap, press and slide on the surface of the carious tissue, and to diagnose the carious level based on haptic perception feeling. Sometimes, this diagnosis is accompanied by visual inspection of the color of the carious tissues, or by X-ray image. For carious tissues at the interproximal surface of the teeth, the dentist has to rely solely on the haptic perception to detect the boundary as the carious part is completely occluded by the teeth. Besides determining the carious level, the boundary between carious and healthy tissues needs to be identified through sliding the tip of the probe from the carious part to the healthy part. For severe decays, when the dentist slides the dental probe from the carious tissue to the healthy tissue, the probe's tip could be stuck at the boundary because of the stiffness difference.

The second step is to explore the internal properties of the caries, i.e., to determine the depth of the carious tissue and to examine the material distributions inside a 3D volume within the target tooth. Depending on the invasive depth, caries can be classified as mild decay (caries limited in enamel), moderate decay (caries affect enamel and superficial dentin) and severe decay (caries affect enamel and reach the deep layer of dentin). The dentist needs to insert a sharp probe into the carious tissue and determine the depth of the

- *D. Wang, X. Zhao, Y. Shi, and Y. Zhang are with the State Key Lab of Virtual Reality Technology and Systems, Beihang University, No. 37 Xueyuan Road, Haidian District, Beijing 100191, China. E-mail: {hapticwang, yuru}@buaa.edu.cn, {zhaoxiaohan_buaa, youjiaoshi}@163.com.*
- *J. Hou is with the School and Hospital of Stomatology, Peking University, Beijing 100081, China. E-mail: jxhou@163.com.*
- *J. Xiao is with the Department of Computer Science, University of North Carolina at Charlotte, Charlotte, NC 28223. E-mail: xiao@uncc.edu.*

Manuscript received 9 July 2015; revised 2 Feb. 2016; accepted 9 Feb. 2016. Date of publication 18 Feb. 2016; date of current version 15 June 2016. Recommended for acceptance by H. Iwata.
For information on obtaining reprints of this article, please send e-mail to: reprints@ieee.org, and reference the Digital Object Identifier below.
Digital Object Identifier no. 10.1109/TOH.2016.2531660

1939-1412 © 2016 IEEE. Personal use is permitted, but republication/redistribution requires IEEE permission.
See http://www.ieee.org/publications_standards/publications/rights/index.html for more information.

carious tissue, which is based on the maximum force felt at the bottom of the carious tissue. Material distribution of the internal volume may be homogenous or non-homogenous. Different force-displacement profiles need to be simulated to reflect the material variance.

Haptic perception skills play a crucial role in correct diagnoses about the stiffness, friction, boundary and depth of varied caries with diverse pathological changes. Furthermore, since a probing operation is performed within a narrow oral cavity, collaborated control of the dental probe's posture and insertion/extraction force is required; otherwise, unintentional movement of the probe's sharp tip may produce damages to adjacent healthy soft tissues such as the tongue and gingiva.

Hence, haptic simulation of such operations may provide a useful tool for training novices to perceive the subtle haptic feeling of probing varied caries and master the motor control skills necessary for diagnoses of caries.

1.2 Related Work

Several approaches have been reported on dental simulation involving haptics [4], [5], [6], [7], [8], [9], [10], while only a few of them provided simulation of caries exploration. Thomas et al. developed a training system with Impulse2000, enabling the operator to practice the detection of carious lesions [9]. Yamaguchi et al. evaluated haptic virtual reality simulation with repetitive training as a tool in teaching caries removal and periodontal pocket probing skills. For the caries removal simulation, multilayered models composed of tooth substance, caries, and pulp were developed [10]. While existing work introduced functional implementation of caries exploration, detailed haptic rendering algorithms were not reported.

In a task of diagnosing dental caries, a dentist needs to manipulate a dental probe to slide along the surface of a target tooth, and to detect the location, area, and depth of caries. The technical challenges for simulating caries exploration include simulating various surface properties of decay that are obviously different from those of a healthy tooth, and simulating the penetration behavior of the probe into non-homogenous 3D carious tissues. Moreover, multi-region contacts may occur between the dental tool and oral tissues, as the tool moves within the narrow space of an oral cavity. Improper movement of the dental probe by a novice will lead to frequent contacts. Therefore, efficient haptic rendering algorithms are needed to compute the six-dimensional interaction force and torque caused by such contacts. The simulated scenarios in existing dental simulators did not consider the internal properties of varied pathological caries, and it is still an open problem to fulfill the clinical requirements of training subtle force feelings of handling varied caries.

The main challenge of simulating surface roughness of caries is friction simulation. There has been considerable research on real-time haptic simulation involving friction combining static, Coulomb, and viscous friction models [11], [12]. Karnopp developed a variation of the basic friction model [13] that expanded the static friction zone to small velocities and switches between static and Coulomb friction, depending on defined velocity thresholds. A number of models derived from this approach has been used for friction rendering [14], [15], [16]. A lot of work on friction simulation was defined within the framework of 3DoF haptic rendering, where the haptic tool was modeled as a point.

Extension to 6DoF haptic rendering requires handling of several challenges: maintaining non-penetration between the tool and the object at all possible multi-contact regions, dealing with different physical properties (contact stiffness and friction coefficients) in each contact region, and simulating six dimensional force/torque exerted on the tool etc. Some approaches have been proposed to tackle those challenges, including the penalty-based approaches [17], [18], [19], [20] and constraint-based approaches [21], [22]. Penalty-based approaches can achieve high update rate while at the risk of instability when the number of simultaneous contacts is large. Constraint-based methods can simulate the friction behavior, but the computation cost was high as modeling friction added more constraints to the linear complementarity framework. Special effort, such as parallel computing or intermediate representations, were used to accelerate the computational efficiency of those methods to meet the 1 kHz update rate of haptic rendering [23], [24]. Besides 6-DoF haptic rendering of multi-region contacts between rigid objects, various models for simulating soft tissues have been developed to simulate surgery process [25], [26], [27], even with stick-slip frictional contacts [28]. Virtual fixtures have shown simplicity and effectiveness in fine manipulation [29].

To some extent, simulation of exploration of internal properties of carious tissues is similar to the simulation of incision of needles. Much work has been proposed on simulation of steering a needle into a tissue [30], [31], [32]. The main difference between caries exploration and needle insertion is that the former needs to simulate multi-region contacts between the probe and the environment during the insertion/extraction process. As the dental probe moves within a narrow oral cavity, unexpected collisions between the probe and neighboring oral tissues may occur during the insertion/extraction of the probe to/from the carious tissues. To simulate caries insertion, the contacts between the probe and the environment have to be detected simultaneously with insertion/extraction simulation, while the contacts can be either with another rigid body (e.g., a tooth) or with surrounding deformable tissues (e.g., gums). Therefore, there is a need for new simulation algorithms to deal with those collisions and to constrain the insertion movement of the probe at the same time.

1.3 Contributions of This Paper

In contrast to previous approaches, our method aims to simulate simultaneous insertion/extraction and frictional multi-region contacts without penetration under the constraint-optimization framework based on a consistent representation of objects, a sphere-tree model, while maintain 1 kHz update rate for stable haptic rendering. The contribution of this paper can be summarized as:

- A configuration-based optimization approach to simulate penetration states between a dental probe and carious tissues within a narrow oral cavity, where a *dynamic sphere-tree* is used to constrain the insertion/extraction of the probe within carious tissues along a fixed direction and enables simulation of the insertion/extraction process with additional

a) Thin stripe on the occlusal surface, b) large area on the occlusal surface, c) decay on the interproximal surface

Fig. 1. Example teeth with carious tissues.

contact constraints between the probe and the contacted rigid or deformable objects.

- Experimental validations consisting of objective force signal analysis and subjective user studies to evaluate the fidelity and stability of the approach. Haptic interaction was stable even when frequent switches between sliding and penetration states occurred, and the approach could simulate subtle differences among different caries with varied surface roughness and boundary shapes.

1.4 Organization of the Paper

The remainder of this paper is organized as follows. In Section 2, we introduce qualitative requirements and quantified specifications for haptic simulation of probing caries. In Section 3, we present a configuration-based optimization approach to simulating state-switching of probing operations of caries, taking into account frictional contacts in sliding states and simultaneous contacts with rigid/deformable bodies during the insertion/extraction process. In Sections 4 and 5, we describe experiments including force signal analysis and user studies to validate the stability of the approach in simulating state transitions and exploration of caries. Finally, we present conclusions and future work in Section 6.

2 Modeling of Healthy and Carious Tissues

In this section, we introduce a sphere-tree modeling method for haptic simulation of probing carious tissues.

2.1 Challenges of Modeling Carious Tissues

In order to simulate haptic interactions in the caries diagnosis task, the following parameters are considered for modeling the carious tissues:

- Location: as shown in Fig. 1, two typical locations are occlusal surface (i.e., contacting surface between corresponding tooth on the lower and upper mandible) and interproximal surface (i.e., contacting surface between two adjacent teeth on the same mandible) in the tooth with carious tissues;
- Shape: the area of the caries can be a thin stripe or a large area with an irregular boundary (Fig. 1b);
- Depth: the depth of the caries, reflecting the severity;
- Material distribution of the internal volume: homogenous or non-homogenous. In the latter case, the stiffness of the caries can either gradually increase or gradually decrease from the top to the bottom of the volume;
- Surface property of caries: isometric or non-isometric frictional behavior.

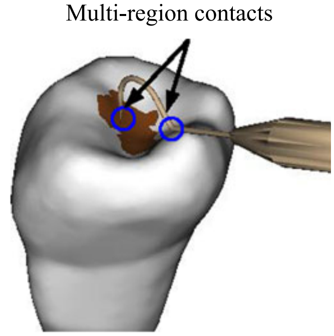

Fig. 2. Multi-region contacts between the probe and oral tissues.

A unique challenge is to simulate the switch between the interaction states of insertion and extraction during the exploration of internal properties. When the probe is penetrated into the carious tissue, it is constrained to only translating along the axis of the probe' tip segment. When the probe is extracted from the carious tissue, there is a resistance force to provide a damping effect. Only when the active force is greater than a threshold, can the probe be extracted from the carious tissue.

During the process, multiple contacts can also occur. As shown in Fig. 2, the probe may simultaneously contact caries and neighboring healthy tissues. The simulation algorithm needs to detect and simulate multi-region contacts between the probe and the oral environment.

2.2 Sphere-Tree Model for Healthy and Carious Tissues

Representing an object with arbitrary shape by a sphere-tree model offers much flexibility and simplifies collision detection, formulation of contact constraints, and deformation modeling [33], [34]. By defining different stiffness and friction coefficient for each sphere, we further extend this model to simulate caries. We construct separate sphere-tree models for the carious tissue and the healthy tissue of a tooth. Fig. 3 shows sphere-tree models of caries on a tooth. By using a detailed level sphere-tree (e.g., level 4 with 4096 spheres), fine geometrical features on the surface of a tooth can be approximated.

Each sphere in the sphere-tree model of the carious tissue is associated with a stiffness parameter and a set of friction coefficients, while the values of these parameters are obtained from empirical data from real dental operations. Diverse caries with various surface roughness, various

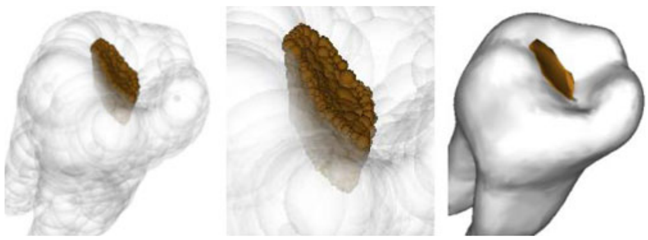

(a) (b) (c)

Fig. 3. Separate sphere-tree models to simulate carious and healthy tissues, respectively, where the spheres in dark brown color denote the carious tissue and the white color denote the healthy tissue: a) a carious volume with a large surface area and an inverted cone shape; b) enlarged view; and c) triangle mesh model for graphic display.

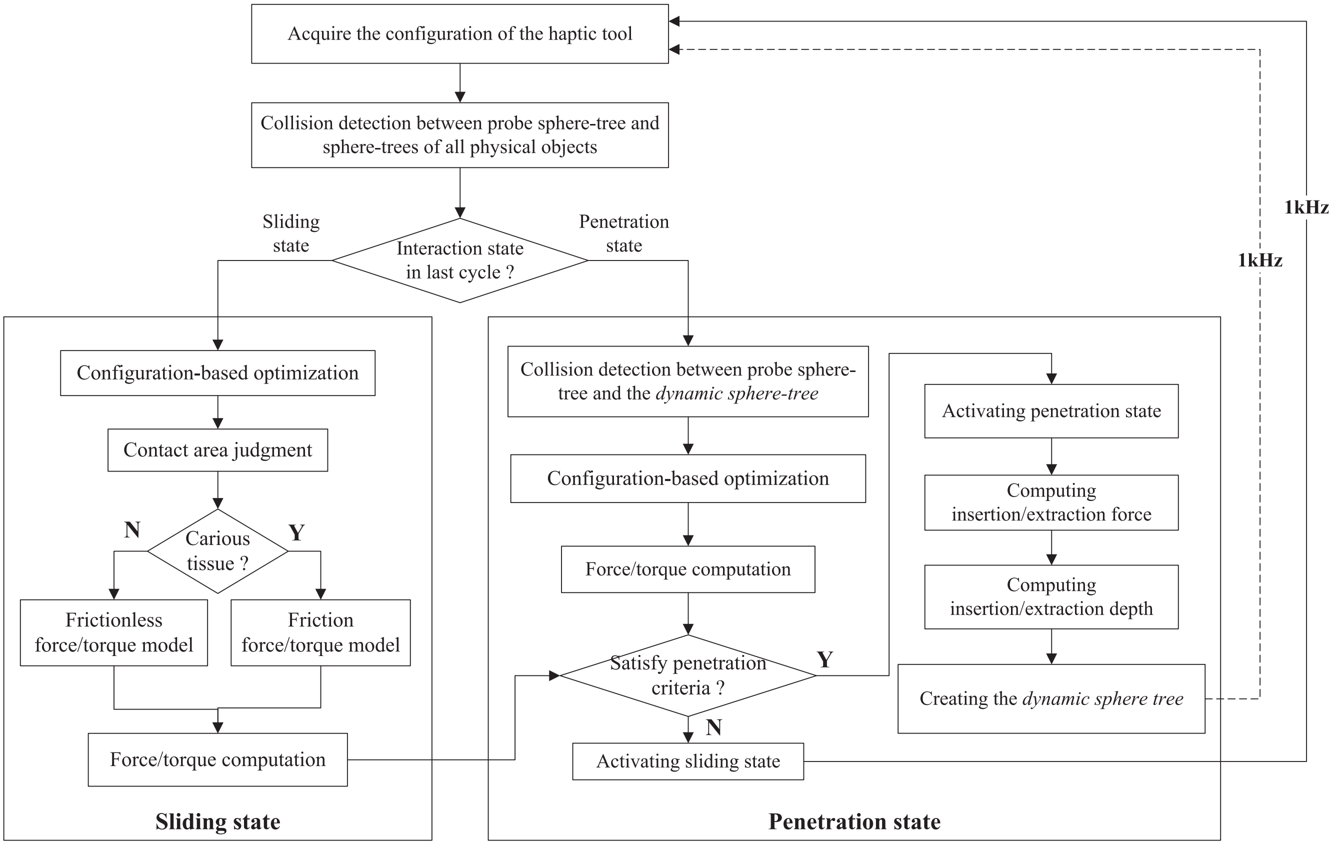

Fig. 4. Configuration-based optimization approach for simulation of state-switching for caries exploration.

depths, and homogenous and non-homogenous tissues could be modeled using the proposed sphere-tree model, with values of the physical parameters determined based on some typical cases of caries in real dental operations. In order to model non-homogenous carious tissues, stiffness and friction coefficients among the spheres that model the caries are set at different values. Also, the gradient between the physical parameters of the healthy and carious tissues influences the difficulty of diagnosis. The greater the gradient, the easier the user can detect the boundary between the carious and healthy tissues.

3 A State-Switching Simulation Approach

In this section, we introduce a state-switching approach to simulate 6DoF haptic interaction of dental probing to explore the surface roughness and internal properties of dental caries.

3.1 Overview of the Approach

The capability of modeling multi-region contacts is a fundamental requirement for 6-DoF haptic simulation systems. The uniqueness of the simulation of caries exploration is to simulate the hybrid contacts consisting of contacts during insertion along the insertion/extraction path and contacts without penetration. The former refers to the contacts between the probe's tip and the caries tissues during insertion/extraction, while the latter refers to the contacts between the probe's body and the surface of adjacent oral tissues. These two types of contacts possess different values of physical parameters, i.e., the internal properties of the caries tissue and surface properties of the adjacent oral tissues are very different. Therefore, it is a novel task and challenge to introduce a unified modeling approach for these two types of contacts and integrate them in the configuration-based optimization framework

As shown in Fig. 4, the state-switching approach models interaction state transitions through checking the contact information between the tool and the tooth and focuses on simulating two kinds of states and their transitions: a sliding state and a penetration state. The two states are designed to simulate surface exploration and internal exploration of dental caries respectively.

In a sliding state, a user moves the dental probe to slide along the surface of a target tooth to detect whether carious tissues exist, and the main simulation requirement is to simulate different tactile feeling from sliding along different tissues, especially different stiffness and friction on the carious tissues. In a sliding state, the tool can freely move in the 3D space and make a single contact or multiple-region contacts with the tooth or nearby oral tissues including neighboring teeth, gingiva, tongue and cheek, etc.

In a penetration state, a user inserts the tip of the dental probe into the internal region of carious tissues to measure the depth and the internal properties including the stiffness and friction of the carious tissues. Four different behaviors need to be simulated within this state:

- Insertion, which requires computing the resistance force and the motion of the dental probe during the insertion process. The probe is constrained to move along a straight-line path into the carious tissue.

- Constrained rotation, which requires simulating the torque feedback to the operator's hand when a voluntary rotation is conducted during the insertion process.
- Extraction, which requires simulating the extraction from the carious tissue. A pulling force needs to be rendered to simulate the damping effect when the user tries to retreat the probe from the caries.
- Additional contact, which requires simulating collisions between the probe and the surface of the tooth and/or adjacent oral tissues, as the probe moves within the narrow oral cavity.

Penetration criteria are defined to trigger the switch to a penetration state, including (1) the tip of the probe must contact the carious tissue and (2) insertion force along the axis of the probe's tip must be greater than a pre-defined threshold. As outlined in Fig. 4, when the penetration criteria are satisfied, a penetration state is activated; otherwise, a sliding state is activated. The threshold is dependent on the modeled pathological degree of the caries: a mild decay has a large value and a severe decay has a small value.

For a penetration state, an extraction criterion is defined to trigger the transition between insertion and extraction sub-states. The insertion state remains until the probe is actively extracted from the caries.

In the following Sections 3.2 and 3.3, the models for simulating the two states are explained in detail.

3.2 Configuration-Based Optimization Approach for Sliding State Simulation

In our previous work [33], we introduced a configuration-based optimization model to solve for the configuration of the *graphic tool*, which is the virtual avatar of the actual *haptic tool*, and to compute the contact normal force/torque to the tool. The optimization is:

$$\begin{cases} Minimize: f(\mathbf{q}_g^t, \mathbf{q}_h^t) \\ Subject\ to: V_O \cap V_T = \varnothing. \end{cases} \tag{1}$$

In equation (1), the objective function $f(\bullet)$ is a distance metric to describe the difference between configurations of the haptic tool and the graphic tool [33]. $\mathbf{q}_h^t$ and $\mathbf{q}_g^t$ are the configurations of the haptic tool and its corresponding graphic tool in the current simulation loop or time step t.

Based on collision detection between the sphere-tree of the tool and the tooth, non-penetration constraint inequalities are formulated, and then a configuration-based optimization is performed to compute the configuration of the graphic tool.

Contact area detection is performed to determine whether the probe is contacting a carious tissue or a healthy tissue. If a healthy tissue is contacted, the frictionless force and torque $\mathbf{F}$ can be derived using the following model

$$\mathbf{F} = G\left(\mathbf{q}_g^t - \mathbf{q}_h^t\right). \tag{2}$$

If the probe is contacting a carious tissue, the configuration-based optimization model is used to compute friction force and torque [35]. Given the known configuration of the graphic tool at the previous and current time steps t-1 and t, and the known haptic configuration of the tool at t, the model could compute static and dynamic frictional force and torque between the dental probe and the surface of carious tissues.

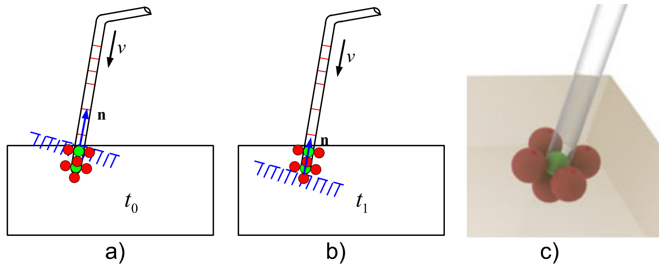

Fig. 5. A red "virtual tunnel" constraint with a moving bottom and changing depth: a) construction of the *dynamic sphere tree;* b) movement of the bottom; and c) 3D illustration of the "virtual tunnel".

As the surface of the carious tissue may consist of anisotropic structures [36], it is a challenge to model the fine detailed surface properties of caries. In our approach, we proposed to use coulomb friction force model with varied fictional coefficient for varied caries. In the next step, it is a possible solution to model texture force using stochastic modeling approaches [37] or using data-driven approaches [38].

3.3 Configuration-Based Optimization Approach for Insertion/Extraction Simulation

In this section, we introduce a configuration-based optimization approach to simulating insertion/extraction when different interactions between the probe and the environment can occur at the same time, i.e., the probe can perform insertion or extraction of caries but can also contact nearby teeth or other tissues in the process due to the narrow space for maneuvering.

3.3.1 A "Virtual Tunnel" Constraint for Defining the Insertion or Extraction Path

The cause of caries is bacterial break down of the hard tissues of the teeth (enamel, dentin and cementum). The minerals in the hard tissues are constantly undergoing processes of demineralization and remineralisation. Dental caries are formed when the demineralization rate is faster than the remineralisation and there is net mineral loss [36]. As revealed by a light microscope, enamel caries consist of several distinct zones including translucent zone, dark zones, body of the lesion, and surface zone [39]. It is difficult or even impossible to exactly model physical properties of caries. Furthermore, diverse pathological changes of the caries may lead to largely different force feelings [36]. The goal of haptic training is to train the correct posture, correct insertion force feeling, and detection of differences among various caries.

We propose a model of a "virtual tunnel" with a moving boundary to determine whether the tip can penetrate into the surface of a carious tissue, the insertion path, and depth of the probe within the carious tissue.

A *dynamic sphere tree* is used to form the virtual tunnel to characterize the insertion path of the probe within the carious tissue. As shown in Fig. 5a, the green sphere denotes the tip of the probe (i.e., the graphic tool). At the contact point between the tip of the probe and the carious tissue, one red sphere is created along the axis $\mathbf{n}$ of the probe's head segment, which is also the direction of insertion, while four other red spheres are created around the head of the probe. We fix the direction **n** once an insertion process starts to simulate the constraint of the tissue on the probe until the probe is completely extracted from the carious tissue. Fig. 5c shows a 3D illustration of the "virtual tunnel" constraint.

The model for computing the insertion force along the direction **n** is as follows:

$$\mathbf{F}_p = -(\mathbf{F}_c \cdot \mathbf{n})\mathbf{n}, \tag{3}$$

where $\mathbf{F}_p$ denotes the insertion force from the probe upon the carious tissue, and

$$\mathbf{F}_c = k_e\left(\mathbf{p}_h^t - \mathbf{p}_g^{t-1}\right), \tag{4}$$

where $\mathbf{F}_c$ denotes the contact force between the probe and the carious tissue. $\mathbf{p}_h^t$ denotes the position vector of the haptic tool in the current simulation cycle, and $\mathbf{p}_g^{t-1}$ denotes the position vector of the graphic tool in the previous simulation cycle. k_e denotes the contact stiffness of the non-homogenous tissue at the contact point.

As stated in Section 3.1, when the penetrating force $\mathbf{F}_p$ is greater than a pre-defined threshold, the probe can insert into the caries. An allowable insertion depth is computed based on the penetration stiffness of the non-homogenous tissue k_c, which is much larger than the value of k_e. Incremental insertion depth in the current simulation cycle is modeled as follows:

$$\begin{cases} \frac{\Delta^t = \mathbf{F}_p}{k_c} & \left\|\mathbf{F}_p\right\| > F_p^* \\ \Delta^t = 0 & \left\|\mathbf{F}_p\right\| \le F_p^*, \end{cases} \tag{5}$$

where F_p^* denotes a pre-defined force threshold needed to overcome before penetrating into the carious tissue.

Along with the increasing insertion depth during the insertion process, the virtual constraint is updated to allow insertion of the graphic tool into the carious tissue. As shown in Fig. 5b, the positions of the five red spheres are updated to simulate the evolving constraint during the insertion process.

Although the mathematical models for computing forces/torques are simple, they capture essential biomechanical behaviors of carious insertion process. First, the insertion movement can be robustly constrained along the insertion path, while diverse force profiles of various pathological changes can be simulated. By adjusting the parameter k_e in equation (4), we can simulate the contact stiffness between the probe and the caries. This enables us to simulate diverse constraints that allow the probe to deviate from the insertion path.

Second, by adjusting the parameter k_c in equation (5), we can simulate the diverse penetration stiffness between the probe and the caries. This enables us to simulate diverse caries from very difficult to very easy to be inserted. The parameter k_c in Eq. (5) can be a constant, a discrete variable that changes value according to insertion depth, or a continuous variable. As shown in Fig. 6, these cases are corresponding to three different types of carious tissues: homogenous tissue caries in the enamel layer, double layers

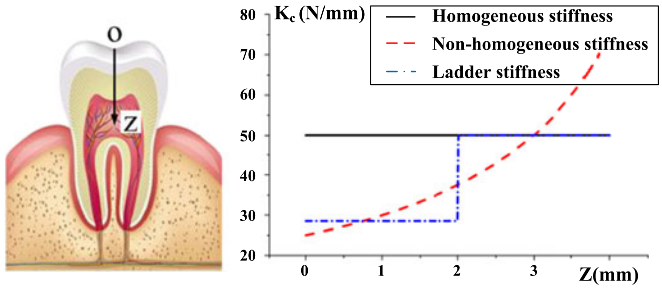

Fig. 6. Profiles of the stiffness versus the insertion depth for three types of caries.

of homogenous caries in the enamel and dentin layers, and non-homogenous caries. The profiles of the stiffness versus the insertion depth are plotted for the three typical types of pathological cases encountered in clinical dental operations.

Furthermore, the force threshold F_p^* can be adjusted to simulate caries with different degrees of pathology. A large value refers to mildly carious tissues and a small value refers to severely carious tissues. By adjusting the parameter F_p^*, we can simulate the diverse breakthrough force between the probe and the caries. To determine the parameters for simulating different levels of typical caries: mild, medium, and severe caries, user study by the dentists were performed and these parameters were tuned from the average feeling of dentists to differentiate hard and soft caries.

3.3.2 Force and Torque Feedback During Insertion Process

During the insertion, the graphic tool of the probe is constrained along the path by the "virtual tunnel". We use the configuration-based optimization model to compute the configuration of the graphic tool and the feedback force/torque based on the configuration of the haptic tool [27]. Therefore, any deviation from the path vector **n** due to the movement of the haptic tool may lead to feedback force and/or torque.

As the graphic tool is constrained to moving along the path vector **n**, the 3D feedback force to the haptic device is computed as follows:

$$\mathbf{F} = k_p^t\left(\mathbf{p}_g^t - \mathbf{p}_h^t\right), \tag{6}$$

where p_g^t and p_h^t denote the three translational components of the configuration variable of the graphic tool and haptic tool. k_p^t denotes the stiffness of the "virtual tunnel" to constrain the motion of the probe, which is set as the maximum value of the associated haptic device to provide a strong constraint.

When a rotation of the haptic tool is detected during the insertion process, the graphic tool will be constrained from rotating by the "virtual tunnel", and the feedback torque is computed as follows:

$$\tau = k_\theta\left(\theta_g^t - \theta_h^t\right), \tag{7}$$

where θ_g^t and θ_h^t denote the orientation vector in terms of Euler angles of the graphic tool and haptic tool respectively. k_θ denotes the rotational stiffness of the non-homogenous tissue.

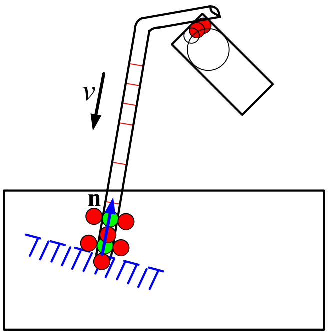

Fig. 7. Additional contacts during insertion.

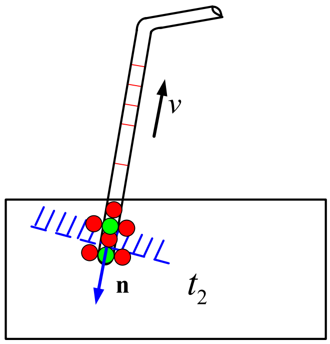

Fig. 8. “Virtual tunnel” during extraction.

3.3.3 Model for Simulating Additional Contacts

If any parts of the probe collide with the target or adjacent tooth and surrounding tissues during the insertion process, the graphic tool of the probe should be constrained by additional contacts. In order to simulate this behavior, collision detection is continuously performed between the sphere-tree of the graphic tool and the sphere-tree of the related teeth and all oral tissues during the insertion process, using the collision detection algorithm introduced in [28].

The collision detection algorithm reports additional intersecting spheres due to collision (Fig. 7), and those spheres are then added to the constraint equations of the configuration-based optimization model.

Under this situation, the user can adjust the posture of the probe to break the unintended collision and re-insert the probe into the carious tissue.

3.3.4 Model for Simulating Extraction Behavior

If the operator intentionally pulls the haptic tool out of insertion, i.e., moving along the opposite direction of the normal $\mathbf{n}$, the following model is introduced to simulate the extraction behavior. A “virtual tunnel” in the opposite direction along $-\mathbf{n}$ is defined to simulate the constraint on the extraction process, as shown in Fig. 8. The “virtual tunnel” becomes shorter and shorter as the extraction proceeds and finally disappears when the probe is completely extracted.

The model for computing extraction force $\mathbf{F}_e$ is similar to that for the insertion force, except that $-\mathbf{n}$ is used

$$\mathbf{F}_e = -(\mathbf{F}_c \cdot \mathbf{n})\mathbf{n}. \tag{8}$$

The model for computing the displacement $\mathbf{p}_s$ of the probe during extraction is as follows:

$$\begin{cases} k_e = 0 & \|\mathbf{F}_e\| > F_e^* \\ \mathbf{p}_s(k) = \mathbf{p}_s(k-1) & \|\mathbf{F}_e\| \leq F_e^* \end{cases}, \tag{9}$$

where the first condition denotes when the extraction process can start. F_e^* denotes a pre-defined force threshold needed to be overcome before the probe can be extracted from the carious tissue. When the probe is successfully extracted from the caries, the operator will feel a sudden drop of feedback force and/or torque.

4 Simulation of Surface Roughness

The purpose is to validate the capability of the proposed approach to simulate various carious tissues with varied frictional coefficient, through objective data analysis and user study. Furthermore, the fidelity of the approach for simulating tissue boundary is evaluated.

4.1 Evaluation on Simulation of Various Roughness

In this section, we present evaluation experiments to validate whether the proposed approach can simulate diversified roughness of various pathological caries. We first analyze the force signals under different friction levels, and then we present a user study to validate the force feeling. In Sections 4.1.1 and 4.2.1, the experiments were simulated based on a computational model, while in Sections 4.1.2 and 4.2.2, the experiments were performed using a haptic device.

4.1.1 Quantified Analysis of Force Signals

We performed evaluations based on objective data to reflect influences of key parameters and contact states on the friction force signals.

To compare the force signals under a given consistent input, we defined a 1-D path of the haptic tool (Fig. 9). The tip of the tool penetrated into the cuboid for 0.59 mm along the path. The trajectory of the haptic tool was then fed into the configuration-based optimization approach to compute the feedback force/torque and the corresponding path of the graphic tool.

In order to understand the different effects of static friction coefficients in the proposed force model, we compare the force signal along x-axis under four levels of static friction coefficient μ_s in Fig. 10, while the dynamic friction coefficient μ_d is fixed as 0.3. From the results, we can observe obvious influences of the static friction coefficient on the friction force signals, i.e., the magnitude of the friction force increased significantly along with the increase of the static friction coefficient. From the friction force signal, we can also observe periodic saw teeth waves, caused by the discontinuous changes of the configuration of the graphic tool.

Similarly, the dynamic friction coefficient was varied to observe its effect on the friction force. The data in Fig. 11 illustrate the friction force signal along x-axis under four values of dynamic friction coefficient, while the static

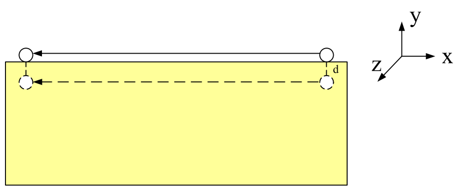

Fig. 9. Pre-defined 1-D path for the haptic tool.

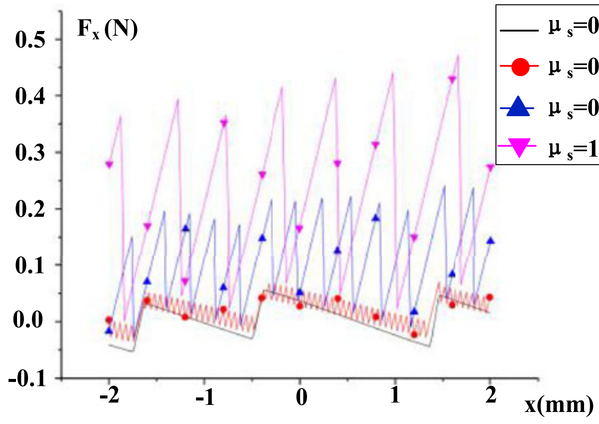

Fig. 10. Force signals as the static friction coefficient changes.

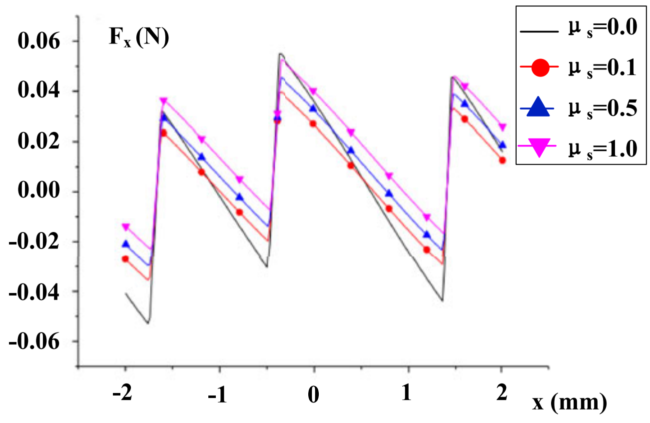

Fig. 11. Force signals as the dynamic friction coefficient changes.

friction coefficient is fixed at 0.5. The results show that the value of the dynamic friction coefficient had only small influence on the friction force signals, i.e., the magnitude of the friction force increased slightly along with the increase of the dynamic friction coefficient.

The above results validate that the proposed approach can simulate versatile friction feelings through tuning of the static and dynamic friction coefficients.

4.1.2 User Study on Roughness Ranking

A Phantom Premium 3.0–6DoF was used in the user study experiment. The device could maintain a simulated stiffness of 1 N/mm throughout its workspace, the maximum output force is 22 N, and the position sensing resolution is 0.02 mm.

Five dentists were invited to perform the caries exploration and thus to determine the parameters of surface roughness. We asked the dentists to slide the virtual probe along the surface of the caries, and to select acceptable values for the static and dynamic friction coefficients to match their haptic sensation to two levels of roughness, i.e., a mild carious tissue with low surface roughness and a severe carious tissue with large surface roughness. The values of the friction coefficients were tuned in a continuous way by a slider on the graphic user interface of the simulation software. Each dentist performed four trials to test the low or the high roughness level. In each trial, a dentist was asked to slide the dental probe through a sequence of two caries with either a low or a high roughness level, where the order of the two levels in the sequence varied from trial to trial. As illustrated in Table 1, the mean and standard deviation of the static and dynamic friction coefficients during the four trials of the five dentists were obtained. Statistical analysis was performed using one-way ANOVA to observe the effect of caries degree on the friction coefficients. For the μ_s, significant difference was observed between the mild caries and severe caries with $F(1, 8) = 14.496$, $p < 0.05$. For the μ_d, a significant difference existed between the mild caries and severe caries with $F(1, 8) = 11.875$, $p < 0.05$. The results illustrate that the proposed approach was able to assist the dentists to tune their preferred values to differentiate mild and severe caries based on their clinical haptic sensations. For all dentists, the values of the friction coefficients of severe caries were greater than those of mild caries. However, the preferred values of the five dentists varied considerably. This might be caused by different haptic perception skills of the dentists. A future topic of study could be on how such variance are influenced by the clinical experiences of different dentists. In our following experiments, we adopted the average values of friction coefficients from the five dentists to simulate roughness exploration operations.

4.2 Evaluation on Simulating Tissue Boundary

In this experiment, the purpose was to validate the effectiveness of the proposed method to simulate various shapes of the boundary between carious and healthy tissues, through both objective data analysis and user study.

4.2.1 Quantified Analysis of Force Signals

During a dental operation, the gradient of the tangential force across the tissue boundary may provide important cues for the user to determine the area or shape of the carious tissue. Computed friction force signals were recorded when a user moved the Phantom haptic device to control the haptic tool sliding from non-frictional to frictional regions along the surface of a virtual cube, or sliding in the opposite direction. Fig. 12 shows the friction force when the haptic tool moved along the axis-x on the surface of a cube. In this scenario, the stiffness of healthy tissues was set to be equal to that of the caries (i.e., 1 N/mm). The magnitude of the friction force in the frictional region was much higher than that of the non-frictional region, and a clear jump of the signal could be observed when the probe came across the boundary.

TABLE 1
Mean and Std. of the Tuned Values of the Friction Coefficients from the Four Trials of Each Dentist

Subjects	Mild caries		Severe caries	
	μ_s	μ_d	μ_s	μ_d
S1	0.06 ± 0.04	0.08 ± 0.04	0.21 ± 0.16	0.16 ± 0.08
S2	0.28 ± 0.17	0.24 ± 0.09	0.51 ± 0.16	0.47 ± 0.15
S3	0.19 ± 0.05	0.19 ± 0.07	0.54 ± 0.09	0.52 ± 0.08
S4	0.17 ± 0.07	0.21 ± 0.06	0.65 ± 0.02	0.60 ± 0.02
S5	0.19 ± 0.03	0.15 ± 0.04	0.64 ± 0.08	0.52 ± 0.09
Average	0.18 ± 0.07	0.17 ± 0.06	0.51 ± 0.16	0.45 ± 0.15

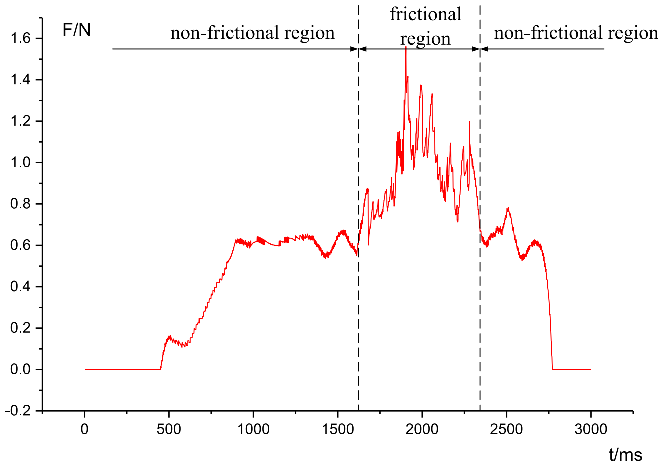

Fig. 12. Friction signal when a user manipulated a virtual probe slide across the boundary between non-frictional and frictional regions.

Furthermore, the gradient of the tangential force across the tissue boundary was also influenced by the stiffness difference between non-frictional and frictional regions. By increasing the stiffness difference between the two regions to a specified value, the probe could be stably hooked at the boundary. This could be used for simulating diagnosis of caries' boundary.

4.2.2 User Study on Identifying 2D Boundaries

In this experiment, we used three target shapes for caries: square, triangle and circle. The caries of those shapes were embedded into the surface of a cube. Fig. 13 shows the geometric models of the three types. It should be noted that the shapes of the caries are not displayed, i.e., the three cubes have the same appearance in the graphic scene. The size of the cube was 100 mm $\times$ 100 mm $\times$ 20 mm. The size of the square was 60 mm $\times$ 60 mm, the length of the triangle is 60 mm, and the diameter of the circle was also 60 mm. The stiffness of both the healthy and carious regions was set as 1 N/mm. The static and dynamic friction coefficients of the carious regions were set as 0.5 and 0.3.

Ten engineering students were invited to attend a perception test to identify the shape of the target boundary. For each participant, ten trials were performed. In each trial, there were three virtual cubes that had the three shapes of boundaries. Each participant was required to slide a virtual probe along the top surface of a virtual cube and to identify the boundary. In each trial, the order of the three boundaries was randomly arranged.

In each trial, the participant was required to identify the boundary shapes. If the participant made a correct identification of all the three shapes, one point was recorded for this trial. Otherwise, zero point was recorded for this trial. Therefore, after ten trials, the possible accumulated score for each participant ranged from 0 to 10. Results show that the mean and standard deviation of the correct rate of the three target shapes is 7.2 ± 1.69.

After the test, the participants were required to fill in a report. All participants reported that clear differences of the friction force signals could be felt when they moved the tool on the surface of the cube across the boundary. They could feel robust hook feeling at the boundary when the haptic tool slided from the frictional region to the non-frictional region.

Fig. 13. The geometric models of three boundaries for detection.

5 Experiments on Probing Caries

In this section, experiments are presented to validate the effectiveness of the proposed method to simulate insertion/extraction process with simultaneous contacts, as well as state transition stability and the effectiveness to simulate typical scenarios of caries for diagnosis.

5.1 Simulating Insertion/Extraction Process with Simultaneous Contacts

Fig. 14 shows the process of insertion/extraction of a dental probe against a cubic pink object with simultaneous non-penetrated contacts with the yellow cubic object. The brown color denotes the graphic tool while the blue color represents the haptic tool. The value of the stiffness k_e, k_c and k_p^t was set as 1 N/mm, 10 N/mm and 1 N/mm, respectively. F_p^* was set as 3 N.

Five phases of the interaction process are illustrated. In the first phase, there was no contact between the probe and the object, therefore the position of graphic tool and haptic tool were collocated. In the second phase, the haptic tool inserted into the carious tissue while the graphic tool stayed on the surface of the carious tissue. As the insertion force had not reached the threshold, the insertion state was not activated yet and the magnitude of inserted depth was zero.

In the third phase, the graphic tool inserted into carious tissue, but had no contact with the adjacent healthy tissue (i.e., the yellow cube). The magnitude of inserted depth gradually increases. In the fourth phase, the graphic tool contacted the healthy tissue. Non-penetration was maintained between the graphic tool and the healthy tissue. In the fifth phase, the graphic tool was extracted from carious tissue. The magnitude of inserted depth gradually decreases, and the feedback force was changed to the opposite direction. In the last phase, the graphic tool was fully extracted from the carious tissue, and the graphic tool and the haptic tool were again collocated.

Except for the fourth phase, the time cost of the haptic rendering cycle was always smaller than 1 ms during all the five phases. In the fourth phase, the time cost of the haptic rendering cycle was slightly greater than 1 ms in some cases.

5.2 Tuning the Parameters for Insertion Operation

The five dentists were invited to perform the caries insertion operation. The dentists insert the virtual probe into the caries, and to select acceptable values for the penetration stiffness and contact stiffness to match their haptic sensation to two levels of stiffness, i.e., a mild decay which is hard to penetrate and a severe decay which is easy to penetrate. The stiffness values were tuned in a continuous way by a slider on the graphic user interface of the simulation software. Each dentist performed four trials to test the low or the high stiffness levels. In each trial, a dentist was asked to insert the dental probe into a sequence of two caries with either a low or a high stiffness level, where the order of the two levels in the sequence varied from trial to trial. Table 2

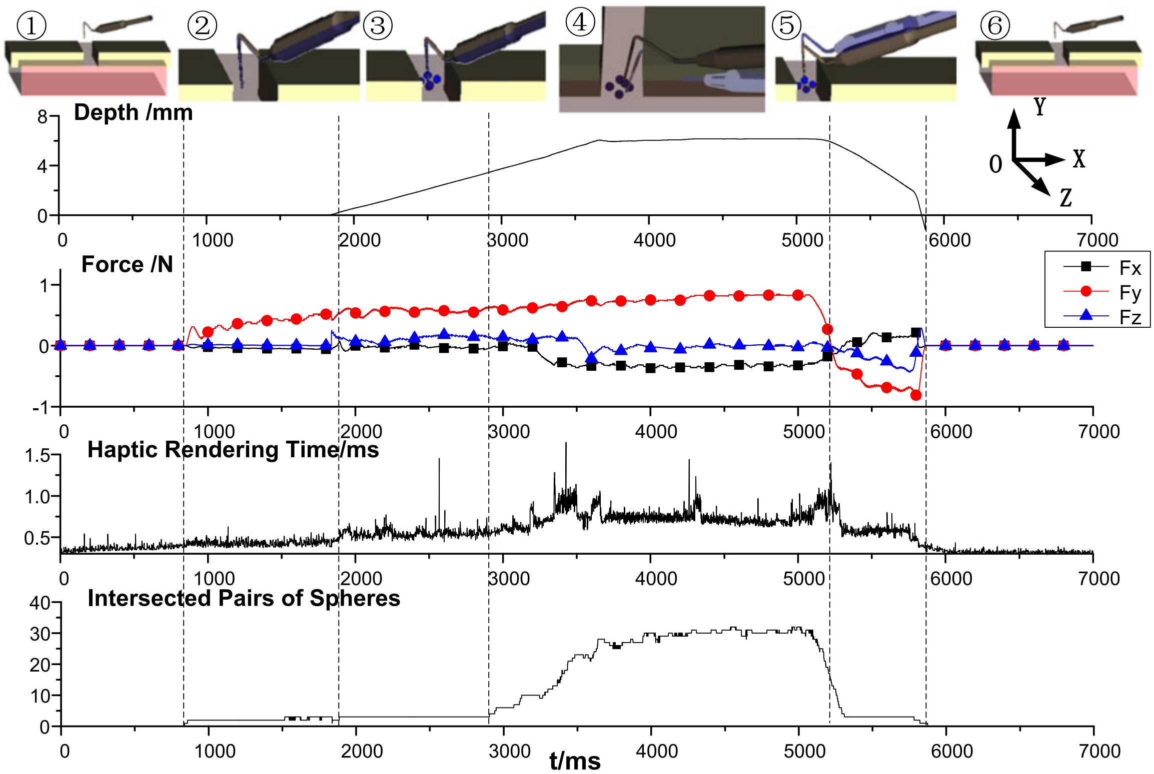

Fig. 14. Five typical phases during an insertion/extraction process: (1) no contact; (2) initial contact without insertion; (3) insertion; (4) insertion with additional contacts; and (5) extraction.

shows the mean and standard deviation for the penetration stiffness and contact stiffness obtained during the four trials by the five dentists. Statistical analysis was performed using one-way ANOVA to observe the effect of caries degree on the stiffness. For the k_c, significant difference was observed between the mild caries and severe caries with $F(1, 8) = 42.124$, $p < 0.05$. For the k_e, no significant difference existed between the mild caries and severe caries with $F(1, 8) = 3.666$, $p > 0.05$. The results illustrate that the proposed approach was able to assist the dentists to tune their preferred stiffness values to differentiate mild and severe caries based on their clinical haptic sensations. For all dentists, the values of the stiffness of severe caries were smaller than those of mild caries. In our following experiments, we adopted the average values of the five dentists to simulate insertion/extraction operations.

With the properly tuned parameter values, the dentists could detect the location and the relative stiffness of the invisible caries through haptic sensation, which demonstrated the feasibility of the model to simulate carious tissues. Furthermore, unintended, additional contacts were robustly simulated when the probe was inserted along an incorrect posture, and thus the trainees could learn to follow correct posture to obtain the maximum insertion depth.

TABLE 2
Mean and Std. of the Tuned Values of Stiffness

Subjects	Mild caries (hard)		Severe caries (soft)	
	k_c	k_e	k_c	k_e
S1	0.38 ± 0.08	0.3 ± 0.0	0.2 ± 0.1	0.37 ± 0.11
S2	0.68 ± 0.04	0.58 ± 0.16	0.18 ± 0.04	0.33 ± 0.04
S3	0.61 ± 0.07	0.53 ± 0.08	0.18 ± 0.08	0.43 ± 0.08
S4	0.60 ± 0.07	0.7 ± 0.14	0.13 ± 0.04	0.5 ± 0.0
S5	0.62 ± 0.04	0.53 ± 0.04	0.3 ± 0.0	0.3 ± 0.08
Average	0.58 ± 0.10	0.53 ± 0.13	0.20 ± 0.06	0.38 ± 0.07

5.3 Integrated Test of Diagnosing Caries

An integrated test of diagnosing caries within an oral cavity was performed by the five dentists to test the effectiveness of the simulation approach. As shown in Fig. 15, two carious regions were modeled in the tooth 46 (i.e., the #1 decay on the occlusal surface, and the #2 decay on the interproximal surface), and the third carious region was modeled in the tooth 36 (the #3 decay on the occlusal surface). In the first step, the color of the carious regions is displayed same as the surrounding healthy regions. The dentists were required to detect the location and the number of carious regions on the two target teeth. In the second step, they needed to judge the relative pathological degree

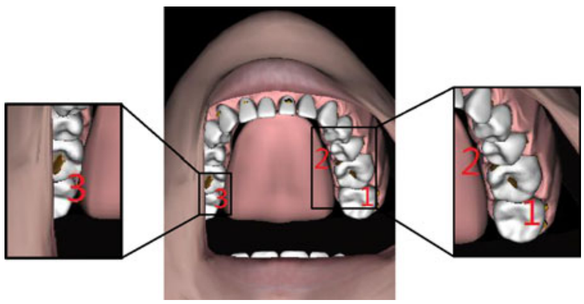

Fig. 15. Two carious regions were modeled in the tooth 46, and one carious regions was modeled in the tooth 36.

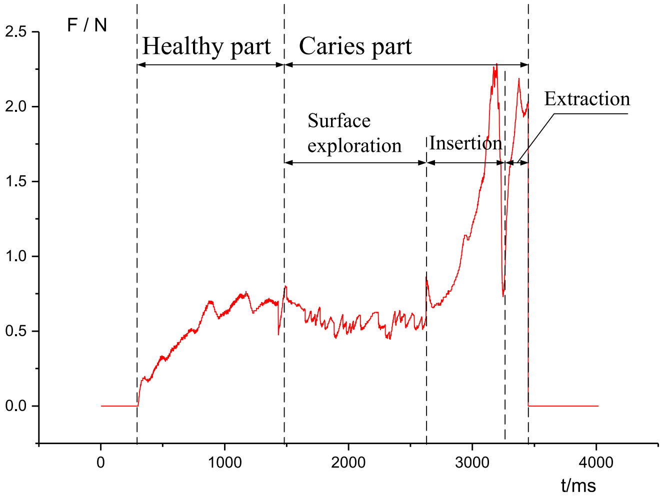

Fig. 16. The normal force signals during different interaction states, while the dashed line illustrates the switching time between two adjacent interaction states.

(i.e., mild or severe caries) of the three carious regions through haptic sensation.

The accuracy of the detection experiments is 100 percent, while the average detection time for each decay was less than 30 seconds. Fig. 16 shows the normal force signal during different interaction states, including sliding along the surface of a healthy tissue, sliding along the surface of a caries, insertion into the caries, and extraction from the caries. The haptic simulation was stable during the whole interaction process. The results validated that frequent state transitions between the sliding and the penetration states could be simulated stably and in real time. Dentists reported that they felt obvious sensations of being stuck at the boundary of invisible caries of the target tooth, which provided important cues for them to diagnose the boundary of the caries.

The accuracy of the stiffness judgment was 60, 40 and 100 percent respectively for the three decays. The possible reason for the differences among the three regions was that the #2 decay on the interproximal surface was difficult to penetrate, as the probe was prone to collide with the neighboring oral tissues when its posture was not correctly controlled.

As shown in Fig. 17a, the caries on the occlusal surface were visible and relatively easy to probe. In Fig. 17b, there were some invisible caries on the neighboring surface, which can only be detected and diagnosed based on haptic sensation. It was challenging to control the fine movement of the dental probe in the narrow oral cavity. Incorrect posture of the dental probe led to collisions between the probe and the tooth, and thus prevented the insertion process. In this case, the operator had to extract the probe and adjust the posture until finding a correct posture for the insertion operation. Frequent contacts occurred during the whole diagnostic test. This shows the necessity of simulating multi-region contacts.

For validation of surgical simulation systems, measurement-based approaches have been used to validate the fidelity of surgical simulation algorithms [40], [41]. In our study, we did not adopt this approach because of two reasons. First, a special probing hardware with force sensing and motion tracking capability need be developed to capture the force-displacement and/or force-velocity profiles during

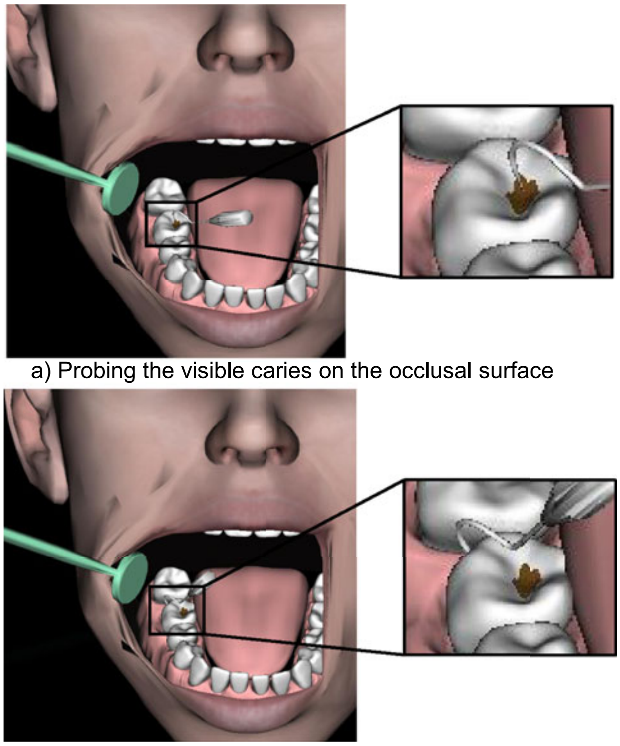

a) Probing the visible caries on the occlusal surface

b) Incorrect posture leads to collisions when probing the invisible caries on the neighboring surface

Fig. 17. Detections of caries in an oral cavity.

manipulation process. Second, and more importantly, it is not safe to perform the in-vivo measurement within the oral cavity of patients. Therefore, we adopted the approach of subjective evaluation to tune the simulation parameter values from user studies. In the next step, one possible solution is to collect carious tissues removed from the target tooth, and perform in vitro measurement using an isolated tooth embedded with the collected carious tissues. In order to perform this study, a large quantity of carious tissue need to be collected as different caries may produce different force-displacement and/or force-velocity profiles.

6 Conclusions and Future Work

In this paper, we have extended our previously proposed configuration-based optimization approach to simulating 6DoF haptic interaction process of exploring the surface roughness and internal properties of dental caries. Diverse caries with various levels of surface roughness, depth, and homogenous and non-homogenous tissues can be simulated using the proposed approach.

To model the 6DoF interaction between a tool and a target tooth, two kinds of interaction states, sliding state and penetration state, are introduced. Penetration criteria consisting of contact states and insertion/extraction force thresholds are defined to trigger the switch between the two states.

To simulate a penetration state, a "virtual tunnel" modeled by a sphere-tree was dynamically created to constrain the movement of the tool within the caries and to compute resistance force during the insertion process. By tuning the stiffness and the force threshold, the model could simulate diverse force feeling of penetrating into homogenous or non-homogenous caries. This model can capture additional contacts between the tool and oral tissues during the insertion/extraction process, which is useful for training the correct postures of the tool in exploring the narrow oral cavity.

Five dentists were invited to perform the caries exploration and the insertion operation. The experimental results illustrate that the proposed approach was able to assist the dentists to tune their preferred friction coefficients and stiffness values to differentiate mild and severe caries based on their clinical haptic sensations. The effectiveness of the approach was validated through an integrated test by the five dentists to diagnose caries within an oral cavity. The results show that the method can provide an integrated environment for training delicate movement of a dental tool within a narrow oral cavity, where multi-region contacts and contact switches frequently occur between the tool and oral tissues.

In the future, we plan to observe the effect of the proposed system on clinical dental skill training and skill transfer.

Acknowledgments

This work is supported by the National Natural Science Foundation of China under the grant No. 61572055, 61532003, 61170187, and 61190125.

References

[1] Y. Yoshida, S. Yamaguchi, Y. Kawamoto, H. Noborio, S. Murakami, and T. Sohmura, "Development of a multi-layered virtual tooth model for the haptic dental training system," *Dental Mater. J.*, vol. 30, no. 1, pp. 1–6, 2011.

[2] R. Santis, L. Ambrosio, and L. Nicolais, "Mechanical properties of tooth structures," *Integr. Biomater. Sci.*, pp. 589–599, 2002.

[3] J. B. Summit, J. W. Robbins, T. J. Hilton, R. S. Schwartz, and J. D. Santos, *Fundamentals of Operative Dentistry: A Contemporary Approach*, 2nd Ed. Carol Stream, IL, USA: Quintessence Publishing, 2001, p. 31.

[4] J. F. Ranta and W. A. Aviles, "The virtual reality dental training system—Simulating dental procedures for the purpose of training dental students using haptics," in *Proc. 4th PHANTOM Users Group Workshop*, Nov. 1999, pp. 67–71.

[5] C. Luciano, P. Banerjee1, and T. DeFanti, "Haptics-based virtual reality periodontal training simulator," *Virtual Reality*, vol. 13, no. 2. pp. 69–85, Jun. 2009.

[6] B. Tse, W. Harwin, A. Barrow, B. Quinn, J. San Diego, and M. Cox, "Design and development of a haptic dental training system - hapTEL,"*Proc. Int. Conf. Haptics Generating Perceiving Tangible Sensations: Part II*, 2010, pp. 101–108.

[7] (2016). [Online]. Available: http://www.moog.com/markets/medical-dental-simulation/haptic-technology-in-the-moog-simodont-dental-trainer/.

[8] J. Forsslund, E. Sallnas, and K. Palmerius, "A user-centered designed FOSS implementation of bone surgery simulations," in *Proc. World Haptics Conf.*, pp. 391–392, 2009.

[9] G. Thomas, L. Johnson, S. Dow, and C. Stanford, "The design and testing of a force feedback dental simulator," *Comput. Methods Programs Biomed.*, vol. 64, pp. 53–64, 2000.

[10] S. Yamaguchi, Y. Yoshida, H. Noborio, S. Murakami, S. Imazato, "The usefulness of a haptic virtual reality simulator with repetitive training to teach caries removal and periodontal pocket probing skills," *Dental Mater. J.*, vol. 32, no. 5, pp. 847–852, Oct. 2013.

[11] P. Buttolo, D. Kung, and B. Hannaford, "Manipulation in real, virtual and remote environments," in *Proc. IEEE Int. Conf. Syst. Man Cybern.*, 1995, vol. 5, pp. 4656–4661.

[12] D. Ruspini, K. Kolarov, and O. Khatib, "The haptic display of complex graphical environments," in *Proc. Annu. Conf. Comput. Graph.*, 1997, pp. 345–352.

[13] D. Karnopp, "Computer simulation of stick-slip friction in mechanical dynamic systems," *ASME J. Dyn. Syst. Meas. Control*, vol. 107, pp. 100–103, 1985.

[14] S. E. Salcudean and T. D. Vlaar, "On the emulation of stiff walls and static friction with a magnetically levitated input/output device," in *Proc. ASME Dyn. Syst. Control Div.*, Chicago, IL, USA, 1994, pp. 303–309.

[15] C. Lee, Y. Lim, and J. Kim, "More physics-based haptic display of frictional virtual surface," in *Proc. IEEE Int. Conf. Control, Autom. Syst.*, Gyeonggi do, South Korea, Oct. 27–30, 2010, pp. 1649–1652.

[16] C. H. Ho, C. Basdogan, and M. Srinivasan, "Efficient point-based rendering techniques for haptic display of virtual objects," *Presence*, vol. 8, no. 5, pp. 477–491, 1999.

[17] M. A. Otaduy and M. C. Lin, "A modular haptic rendering algorithm for stable and transparent 6-DoF manipulation," *IEEE Trans. Robot.*, vol. 22, no. 4, pp. 751–762, Aug. 2006.

[18] J. Barbič and D. L. James, "Six-DoF haptic rendering of contact between geometrically complex reduced deformable models," *IEEE Trans. Haptics*, vol. 1, no. 1, pp. 39–52, Jan 2008.

[19] Y. J. Kim, M. A. Otaduy, M. C. Lin, and D. Manocha, "Six-degree-of freedom haptic rendering using incremental and localized computations," *Presence*, vol. 12, no. 3, pp. 277–295, 2003.

[20] Q. Luo and J. Xiao, "Physically accurate haptic rendering with dynamic effects," *IEEE Comput. Graph. Appl.*, vol. 24, no. 6, pp. 60–69, Nov./Dec. 2004.

[21] C. Duriez, F. Dubois, A. Kheddar, and C. Andriot, "Realistic haptic rendering of interacting deformable objects in virtual environments," *IEEE Trans. Vis. Comput. Graph.*, vol. 12, no. 1, pp. 36–47, Jan. 2006.

[22] M. Ortega, S. Redon, and S. Coquillart, "A six degree-of-freedom god-object method for haptic display of rigid bodies with surface properties," *IEEE Trans. Vis. Comput. Graph.*, vol. 13, no. 3, pp. 458–469, May 2007.

[23] I. Peterlik, M. Nouicer, C. Duriez, S. Cotin, and A. Kheddar, "Constraint- based haptic rendering of multirate compliant mechanisms," *IEEE Trans. Haptics*, Spec. Issue Haptics Med. Clin. Skill Acquisition, vol. 4, no. 3, pp. 175–187, Jul. 2011.

[24] H. Courtecuisse, H. Jung, J. Allard, C. Duriez, D. Y. Lee, and S. Cotin, "GPU-based real-time soft tissue deformation with cutting and haptic feedback," *Progress Biophys. Molecular Biol.*, vol. 103, pp. 159–168, 2010.

[25] S. Suzuki, N. Suzuki, A. Hattori, A. Uchiyama, and S. Kobayashi, "Sphere-filled organ model for virtual surgery system," *IEEE Trans. Med. Imag.*, vol. 23, no. 6, pp. 714–22, Jun. 2004.

[26] C. Paloc, A. Faraci, and F. Bello, "Online remeshing for soft tissue simulation in surgical training," *IEEE Comput. Graph. Appl.*, vol. 26, no. 6, pp. 24–34, Nov./Dec. 2006.

[27] R. Kikuuwe, H. Tabuchi, and M. Yamamoto, "An edge-based computationally efficient formulation of Saint Venant- Kirchhoff tetrahedral finite elements," *ACM Trans. Graph.*, vol. 28, pp. 1–13, 2009.

[28] P. Jacobs and M. C. Cavusoglu, "High fidelity haptic rendering of stick-slip frictional contact with deformable objects in virtual environments using multi-rate simulation," in *Proc. IEEE Int. Conf. Robot. Autom.*, 2007, pp. 117–123.

[29] A. Bettini, P. Marayong, S. Lang, A. M. Okamura, and G. D. Hager, "Vision-assisted control for manipulation using virtual fixtures," *IEEE Trans. Robot.*, vol. 20, no. 6, pp. 953–966, Dec. 2004.

[30] J. Hing, A. Brooks, and J. Desai, "Reality-based estimation of needle and soft-tissue interaction for accurate haptic feedback in prostate brachytherapy simulation," *STAR Robot. Res.*, vol. 28, pp. 34–48, 2007.

[31] D. Lorenzo, Y. Koseki, and E. D. Momi, "Coaxial needle insertion assistant with enhanced force feedback," *IEEE Trans. Biomed. Eng.*, vol. 60, no. 2, pp. 379–389, Feb. 2013.

[32] O. Goksel, K. Sapchuk, and S. E. Salcudean, "Haptic simulator for prostate brachytherapy with simulated needle and probe interaction," *IEEE Trans. Haptics*, vol. 4, no. 3, pp. 188–198, Jul. 2011.

[33] D. Wang, X. Zhang, Y. Zhang, and J. Xiao, "Configuration-based optimization for six degree-of-freedom haptic rendering for fine manipulation," *IEEE Trans. Haptics*, vol. 6, no. 2, pp 167–180, Apr.–Jun. 2013.

[34] D. Wang, Y. Shi, S. Liu, Y. Zhang, and J. Xiao, "Haptic simulation of organ deformation and hybrid contacts in dental operations," *IEEE Trans. Haptics*, vol. 7, no. 1, pp. 48–60, Jan. 2014.

[35] D. Wang, J. Xiao, and Y. Zhang, *Haptic Rendering for Fine Manipulation*. New York, NY, USA: Springer, 2014.

[36] O. Fejerskov, B. Nyvad, and E. A. Kidd, "Pathology of dental caries," in O. FejerskovO, E. KiddEAM(eEds.), *Dental Caries: The Disease and Its Clinical Management*, Oxford, U.K.: Blackwell Munksgaard, 2008, vol. 2, pp 20–48.

[37] J. P. Fritz and K. E. Barner, "Stochastic models for haptic texture," *Proc. SPIE*, vol. 2901, pp. 34–44, 1996.
[38] H. Culbertson, J. Unwin, and K. J. Kuchenbecker, "Modeling and rendering realistic textures from unconstrained tool-surface interactions," *IEEE Trans. Haptics*, vol. 7, no. 3, pp. 381–393, Jul.–Sep. 2014
[39] A. I. Darling, "Resistance of the enamel to dental caries," *J. Dental Res.*, vol. 42, no. 1, pp. 488–96, 1963
[40] S. Misra, K. T. Ramesh, and A. M. Okamura, "Modeling of tool-tissue interactions for computer-based surgical simulation: A literature review," *Presence*, vol. 17, no. 5, pp. 463–491, 2008.
[41] M. P. Ottensmeyer, E. Ben-Ur, and J. K. Salisbury, "Input and output for surgical simulation: Devices to measure tissue properties in vivo and a haptic interface for laparoscopy simulators," *Stud. Health Technol. Inform.*, vol. 70, pp. 236–42, 2000.

Dangxiao Wang received the PhD degree from Beihang University, Beijing, China, in 2004. He is currently an associate professor at the State Key Laboratory of Virtual Reality Technology and Systems, Beihang University, Beijing, China. From 2004 to 2006, he was a postdoctoral fellow at Beihang University. From 2006 to 2007, he was an assistant professor in the School of Mechanical Engineering and Automation, Beihang University. His research interests include haptic rendering, neurohaptics, and medical robotic systems. He has been the chair of Executive Committee of the IEEE Technical Committee on Haptics (IEEE TCH) since 2014. He is a senior member of the IEEE.

Xiaohan Zhao received the BE degree in mechanical design from the School of Mechanical Engineering & Automation, Beihang University, Beijing, China, in 2014. He is currently working toward the ME degree in mechanical engineering at the Beihang University, Beijing, China. His research interests include mechanism design and haptic rendering.

Youjiao Shi received the BE degree in mechanical design from the Najing University of Aeronautics and Astronautics, Nanjing, Jiangsu Province, China, in 2012. She is currently working toward the ME degree in mechanical engineering at the Beihang University, Beijing, China. Her research interests include haptic rendering.

Yuru Zhang received the PhD degree in mechanical engineering from Beihang University, Beijing, China, in 1987. She is currently leading the Division of Human-Machine Interaction, State Key Laboratory of Virtual Reality Technology and System. Her technical interests include haptic human-machine interface, medical robotic system, robotic dexterous manipulation, and virtual prototyping. She is a senior member of the IEEE and a member of the ASME.

Jianxia Hou received the DDS and MS degrees from Xi'an Jiaotong University, School of Stomatology, China, in 1994 and 1999, respectively, and the PhD degrees from Peking University School of Stomatology, Beijing, China, in 2001. She is currently a clinical professor at Peking University, School and Hospital of Stomatology, China. She is councilor at the Asian Pacific Society of Periodontology. She is also a member of the IADR and the Chinese Society of Periodontology.

Jing Xiao received the PhD degree in computer, information, and control engineering from the University of Michigan, Ann Arbor, MI, USA. She is currently a professor of computer science at the College of Computing and Informatics, University of North Carolina at Charlotte, Charlotte, NC, USA. Her research interests include robotic manipulation and assembly, haptic rendering, and motion planning. She is a fellow of the IEEE.

▷ **For more information on this or any other computing topic, please visit our Digital Library at** www.computer.org/publications/dlib.